



Task-Model Alignment: A Simple Path to Generalizable AI-Generated Image Detection

Ruoxin Chen¹, Jiahui Gao², Kaiqing Lin³, Keyue Zhang¹, Yandan Zhao¹,
Isabel Guan⁴, Taiping Yao¹, Shouhong Ding^{1,†}

¹Tencent Youtu Lab, ²East China University of Science and Technology,

³Shenzhen University, ⁴Hong Kong University of Science and Technology

[†] Corresponding Authors

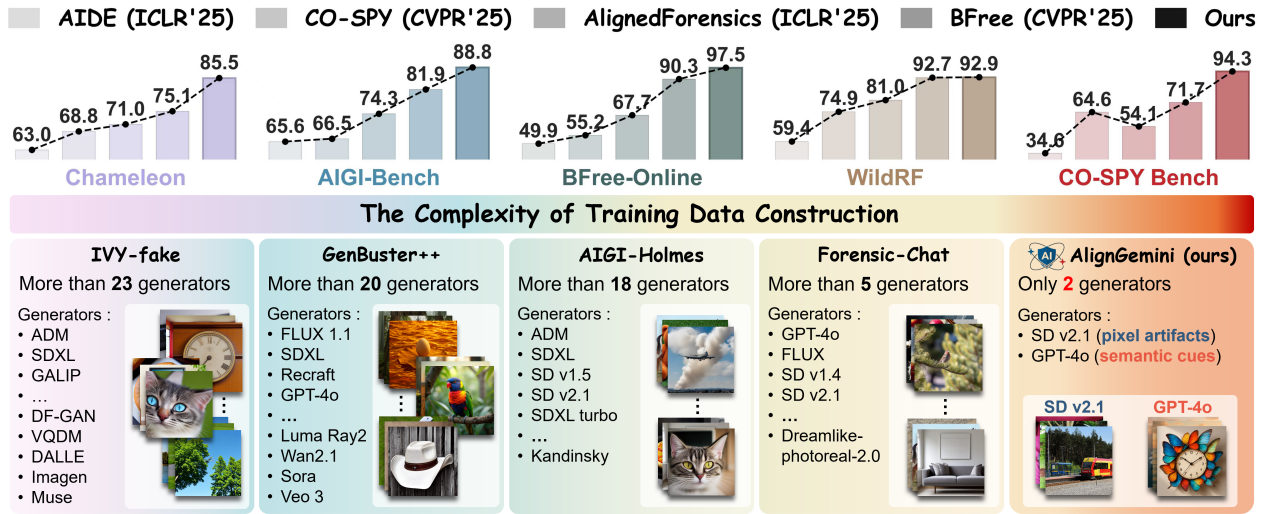


Figure 1. **Top:** Comparison on five in-the-wild benchmarks. **Bottom:** Comparison of dataset construction complexity. Overall, our **AlignGemini** outperforms existing detectors in in-the-wild generalization while relying on a substantially simpler training corpus than other VLM-based detectors, representing a step toward practical deployment.

Abstract

Vision Language Models (VLMs) are increasingly adopted for AI-generated images (AIGI) detection, yet converting VLMs into detectors requires substantial resource, while the resulting models still exhibit severe hallucinations. To probe the core issue, we conduct an empirical analysis and observe two characteristic behaviors: (i) fine-tuning VLMs on high-level semantic supervision strengthens semantic discrimination and well generalize to unseen data; (ii) fine-tuning VLMs on low-level pixel-artifact supervision yields poor transfer. **We attribute VLMs’ underperformance to task-model misalignment: semantics-oriented VLMs inherently lack sensitivity to fine-grained pixel artifacts, and semantically non-discriminative pixel artifacts thus exceeds their inductive biases.** In contrast, we observe that conventional pixel-artifact detectors capture low-level pixel artifacts yet exhibit limited semantic awareness relative to VLMs, highlighting that distinct models are better matched

to distinct tasks. In this paper, we formalize AIGI detection as two complementary tasks—semantic consistency checking and pixel-artifact detection—and show that neglecting either induces systematic blind spots. Guided by this view, we introduce the **Task-Model Alignment** principle and instantiate it as a two-branch detector, **AlignGemini**, comprising a VLM fine-tuned exclusively with **pure semantic supervision** and a pixel-artifact expert trained exclusively with **pure pixel-artifact supervision**. By enforcing orthogonal supervision on two simplified datasets, each branch trains to its strengths, producing complementary discrimination over semantic and pixel cues. On five in-the-wild benchmarks, AlignGemini delivers a **+9.5** gain in average accuracy, supporting task-model alignment as an effective path to generalizable AIGI detection.

1. Introduction

“Know your circle of competence and stay within it.”

The rapid progress of generative models [10, 13, 36, 46] has fueled innovation across creative industries, but the growing volume of AI-generated images has heightened misinformation risks, making detection essential. Recently, VLMs have gained increasing attention, motivating their adaptation for AIGI detection. Early works [4, 41] explore the potential of VLMs, and subsequent studies enhance VLM-based detectors via prompt engineering [15], reinforcement learning [42, 53], curated datasets with fine-grained annotation [42, 49], multi-task supervision [17, 39], reasoning-oriented mechanisms [8, 14, 40], and fusion with expert detectors [4, 28, 34, 53], all aiming to better align VLMs with the task of AIGI detection.

However, *studies have shown that VLM-based detectors suffer from two critical limitations* [9, 19, 43]: (i) VLMs are prone to hallucinations, often producing incorrect labels with fabricated or spurious explanations; (ii) explanation-oriented annotation is intrinsically ill-defined, especially for synthetic images without evident flaws, where annotators are required to provide fine-grained artifact descriptions that are ambiguous and unreliable.

To investigate why VLM-based detectors yield only marginal gains, we conduct *an empirical analysis (Section 3) and observe two characteristic behaviors*: (i) When fine-tuned on high-level semantic supervision, the VLM markedly improves its semantic discrimination and generalizes well to unseen generators; (ii) when fine-tuned on low-level pixel-artifact supervision, the conventional vision backbone achieves strong, generalizable pixel-artifact detection. However, the VLM fails to acquire pixel-level perception, and the conventional vision model struggles to match the VLM’s semantic awareness. Moreover, mixed semantic-and-pixel supervision dilutes each model’s inherent strengths rather than delivering both capabilities. These findings indicate that different models are inherently aligned with different tasks by virtue of their pretraining paradigms and architectures; forcing a model to optimize for a misaligned or mixed objective induces **task-model misalignment** and leads to suboptimal performance.

In this paper, first we show that both semantic and pixel-artifact detection are indispensable for AIGI detection: neglecting either would induce systematic blind spots and large-scale missed detections of synthetic images. (i) Semantic detectors, which rely on implausible content, struggle against content-faithful synthetic images produced by increasingly realistic generators. (ii) Pixel-artifact detectors, which depend on low-level pixel statistics, are brittle under post-processing operations (e.g., resizing, compression), where generation traces can be heavily distorted or removed. Hence, a reliable detector must jointly exploit semantic consistency and pixel artifacts.

Guided by our empirical findings, we propose the **Task-**

Model Alignment principle: *assign model to its native task and train with task-pure supervision targeting the task’s core signal*. We instantiate this principle in AlignGemini, a dual-perspective detector that integrates a VLM specialized for semantic consistency with a conventional vision backbone specialized for pixel artifacts. Our contributions are:

- **Task-Model Alignment Principle and AlignGemini.**

We formalize the **Task-Model Alignment** principle and instantiate it with AlignGemini. The VLM is fine-tuned on a **pure semantic supervision set**, and pixel expert is trained on a *pure pixel-artifact supervision set*. Two training sets are “orthogonal” and align with each model’s strengths. With a simplified corpus, AlignGemini improves five in-the-wild benchmarks by **+9.5** (Figure 1).

- **A Contemporary Benchmark: AIGI-Now.** We construct AIGI-Now, a benchmark spanning nine modern generators—including six commercial closed-source generators—and, for each generator, providing two disjoint subsets: *semantically discriminative* and *pixel-level-discriminative* samples. This design enables a disentangled evaluation of semantic versus pixel-artifact detection capabilities on current-generation AIGI.

2. Related Works

AIGI Detection via Conventional Vision Models. CNNSpot [37] first shows that a vanilla CNN readily detects synthetic images from *seen* generators but fails to generalize to *unseen* ones. UnivFD [27] subsequently improves cross-generator generalization by adopting the VLM model CLIP as a backbone. Follow-up studies [6, 18, 20, 23, 31–33, 45, 50, 52] pursue generalization by redesigning architectures, refining fine-tuning protocols, preprocessing inputs, and tailoring loss functions. Nevertheless, these detectors predominantly rely on low-level artifacts, making them brittle under common post-processing operations such as compression and resizing. Consequently, they may fail to reliably detect semantically implausible synthetic images once low-level traces are suppressed, even though such semantic failures often occur in the most user-salient cases.

AIGI Detection via VLM. VLMs excel at image-text semantic understanding, a capability that remains reliable under common post-processing and helps distinguish semantically implausible fakes, making them attractive for AIGI detection. Early work UnivFD [27] employs the VLM model CLIP [29] as a backbone to improve generalizability, followed by methods [26, 31] that further adapt CLIP for AIGI detection. With the emergence of large VLMs (LVLMs), subsequent studies increasingly rely on scaling datasets and labels: FakeShield [41] aggregates six datasets and, with GPT-4o-annotated defect regions and rationales, performs supervised fine-tuning; FakeVLM [39] builds

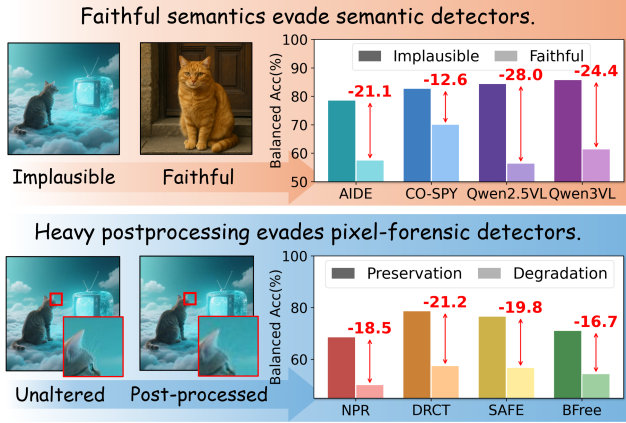


Figure 2. Illustration of blind spots of semantic and pixel-artifact detectors. **Top:** semantically-faithful synthetic images evade semantic detectors despite clear pixel artifacts. **Bottom:** heavy degradations (e.g., compression, resizing) destroy the generation pixel trace, greatly reducing pixel-artifact detectors’ detection rate by 16%+, even for evidently implausible synthetic images.

FakeClue dataset from five sources and employs three pre-trained VLMs for aggregated annotation; IVY-Fake [49], LEGION [17], BusterX++ [38], Forensic-Chat [24], VLM-Defake [15], and AIGI-Holmes [22] further expand coverage across generators, datasets, and forgery types via expert annotations or cross-LLM validation. Overall, current VLM-based detectors prioritize aggressive dataset aggregation and high-fidelity labels, incurring substantial annotation and computational cost while offering uncertain gains in real deployment. A further concern is benchmark overlap (“in-domaining”): when overlapping or closely related generators appear in both training and evaluation, reported improvements may largely reflect memorization rather than genuine out-of-distribution robustness. By contrast, our AlignGemini shows that a simplified corpus with lightweight supervision is sufficient to train complementary semantic and pixel-artifact branches, avoiding such overlap and yielding stronger generalization.

AIGI Detection via VLM with Experts. Extensive work [5, 11, 16, 48] shows that VLMs are weak at fine-grained, pixel-level perception, and are therefore required for external experts. AIDE [44] couples CLIP with a shallow CNN to inject pixel-level cues. CO-SPY [5] fuses CLIP semantic features with VAE reconstruction residuals to capture both semantic and pixel cues. Meanwhile, large VLMs (LVLMs) are adopted to strengthen the semantic branch. X2-DFD [4] augments an LVLM with expert detectors to recover pixel-level signals. AIGI-Holmes [22] pairs an LVLM with CLIP and NPR [7] to integrate high- and low-level signals. AvatarShield [42] concatenates an additional residual module to enhance low-level perception. In summary, external experts can

compensate VLMs’ inherent low-level deficits and enable fusion of semantic and pixel-level signals. However, these experts are typically attached in an ad hoc manner, without a principled scheme to enforce complementarity. Above methods separate semantics and pixels architecturally (e.g., CLIP for semantics, VAE residuals for pixels) but overlook the data perspective: training sets remain mixed—some are semantically non-discriminative, others pixel-non-discriminative—entangling supervisory signals and limiting branch specialization and generalization. A further issue is the prevalent fine-tuning of VLMs on training sets containing **semantically indiscriminate synthetic images**—distinguishable only via pixel cues. We show that such mixed semantic-pixel supervision neither enhances pixel sensitivity nor preserves semantic generalization, ultimately degrading generalizability to unseen generators. In contrast, AlignGemini treats data as the primary lever for shaping model roles and enforces complementarity at the data level: *the VLM is trained on a purely semantic corpus where pixel statistics are perturbed to block low-level shortcuts, while expert models are trained on purely pixel-discriminative synthetic images that match real images in high-level semantics.*

3. Motivation

AIGI Detection as Two Tasks: Semantic and pixel-artifact Detection. AIGI detection fundamentally comprises two complementary tasks: (i) *semantic-consistency verification*—assessing whether image content exhibits semantic flaws; (ii) *pixel-artifact detection*—identifying low-level generation traces. Either task can succeed on particular cases but is susceptible to systematic blind spots, as shown in Figure 2. Semantic detectors are tolerant to common degradations yet can be bypassed by content-faithful synthetic images that preserve plausible semantics. Pixel-cue detectors, while able to capture imperceptible traces, are fragile under post-processing, where simple resizing or compression substantially alters pixel statistics. *Relying on either task alone therefore leaves vulnerabilities, motivating detectors that jointly exploit both semantic and pixel signals.*

An Empirical Analysis of Task-Model Alignment. After establishing that both semantic and pixel signals are necessary, we conduct an empirical analysis to assess how well different models align with semantic and pixel-artifact detection. We construct three distinct supervision sets: (i) *Pixel-artifact set*: synthetic images are generated via VAE reconstruction to be semantically indistinguishable from real images while differing only in pixel statistics, a commonly used technique that injects artifacts while preserving semantics. (ii) *Semantically-implausible set*: synthetic images exhibit semantic inconsistencies generated by GPT-4o

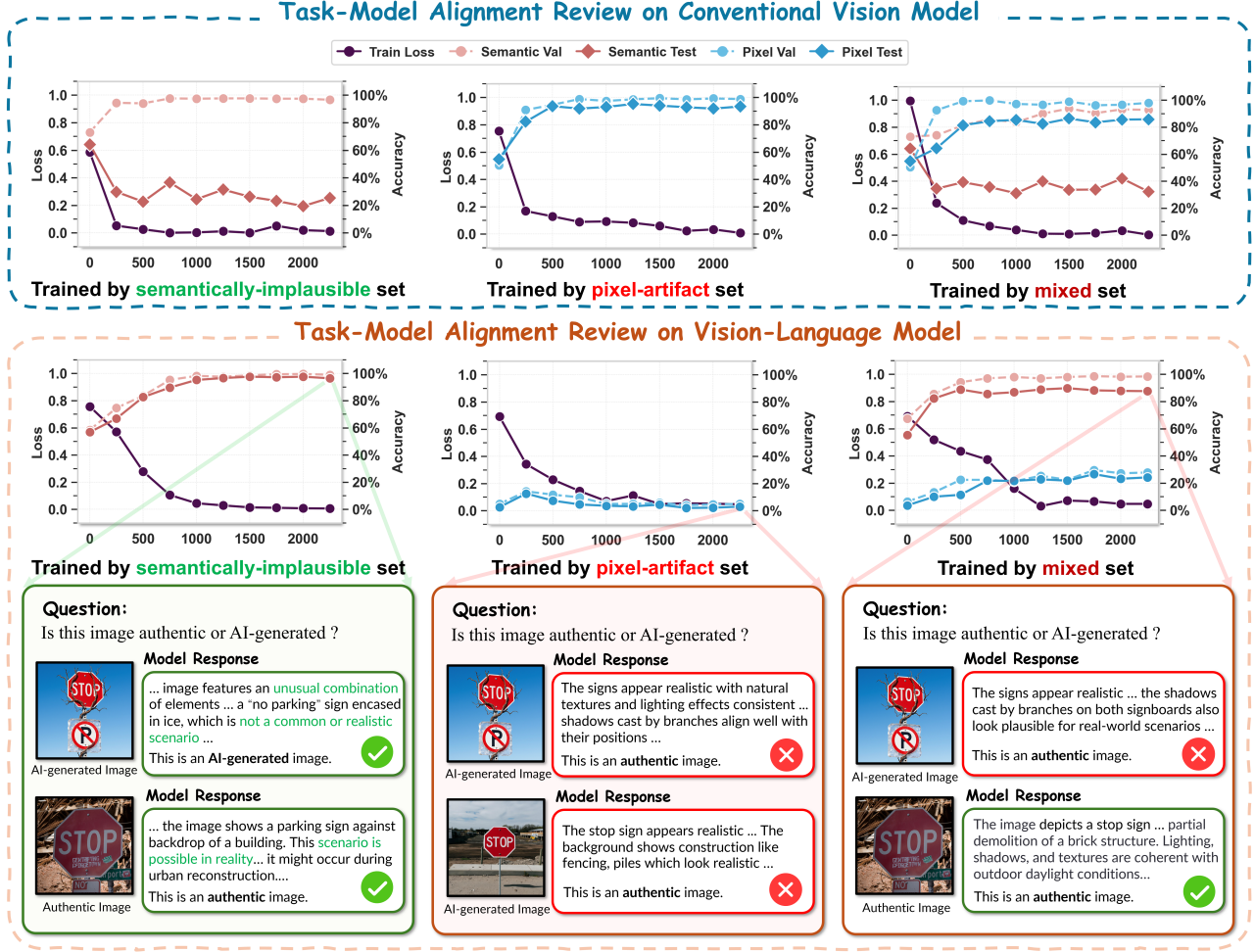


Figure 3. Analyze the performance of a conventional vision backbone (DINOv2) and a VLM (Qwen2.5-VL-7B) under semantic vs. pixel-artifact supervision. “Semantic/Pixel Val” denotes synthetic images generated by the same generator used in training, while “Semantic/Pixel Test” denotes synthetic images from unseen generators. **Top:** DINOv2 trained with semantic supervision generalizes poorly on the semantic test set, whereas DINOv2 trained with pixel-artifact supervision generalizes well on the pixel test set. **Bottom:** Qwen-VL trained with semantic supervision reliably identifies semantic flaws from unseen generators, while pixel-artifact supervision fails to enhance its pixel-artifact detection. **Rightmost Column:** The mixed semantic-pixel supervision undermines each model’s inherent strengths. Together, these results indicate a clear task-model alignment: **conventional vision model is better suited for pure pixel-artifact cues, whereas VLM is better suited for pure semantic cues.**

with surreal prompts, and their pixel statistics are heavily perturbed by aggressive post-processing to suppress low-level shortcuts. (iii) *Mixed set*: a combination of the above two types. We then train a VLM (Qwen-VL) and a conventional vision backbone (DINOv2) on each supervision set and observe three patterns (Figure 3): (i) The VLM inherently excels at detecting semantic flaws, reflecting its large-scale image-text pretraining, and this capability is further strengthened by semantic supervision, generalizing well to unseen generators. However, it remains largely insensitive to low-level pixel artifacts even after pixel-artifact fine-tuning, suggesting a structural limitation in modeling low-level cues. (ii) DINOv2 is strong at identifying pixel artifacts, and its pixel-artifact features generalize well to un-

seen generators. However, it clearly lags behind VLMs in detecting semantic flaws. (iii) Mixed semantic-pixel supervision does not produce a single model that excels at both, but instead dilutes each model’s inherent strengths. The analysis yields a clear takeaway: *VLMs and other models are inductively biased toward different tasks primarily due to their distinct pretraining paradigms. Task-Model Alignment, which assigns each task to its suited model, yields higher cross-generator generalization.*

4. Methodology

To isolate the effect of task-model alignment, we adopt a two-stage pipeline: simplified data construction and lightweight fine-tuning. Our design deliberately avoids



Figure 4. **Comparison between AIGI-Now and existing benchmarks.** **Top:** Existing benchmarks mainly rely on pre-2023 open-source generators. By contrast, real-world usage is dominated by newer commercial, closed-source models, creating a clear gap between the existing benchmark data and real-world fakes. **Bottom:** Our proposed AIGI-Now is constructed from the latest generators (all released after 2024), including six commercial, closed-source models such as GPT-4o with unknown architectures, enabling rigorous evaluation of detectors’ cross-architecture generalization and making the benchmark substantially closer to real-world application scenarios.

heavy curation to promote end-to-end reproducibility.

Purity-First Orthogonal Dataset Construction for Task-Model Alignment. Rather than fine-grained annotations and heavy engineering, we use a simple dataset construction that foregrounds *purity* and *orthogonality*. We build two *orthogonal* supervision sets so that semantic and pixel cues are *disjoint* by construction. (i) The *semantically-implausible* supervision set, used to fine-tune the VLM, pairs natural images with *semantically inconsistent* synthetic images.¹ To prevent leakage of low-level signals, both real and synthetic images undergo identical randomized heavy post-processing, which deliberately perturbs pixel statistics while preserving semantics. We construct Direct Preference Optimization (DPO) supervision by prepending a fixed verdict prefix (“*This is an AI-generated image.*”/“*This is an authentic image.*”) and eliciting two responses per image, forming preferred-dispreferred pairs. We emphasize that this pipeline requires neither a VLM-as-Judge nor human raters, because semantic inconsistencies are salient and VLMs excel at spotting them, the risk of label hallucination is reduced. (ii) The *pixel-artifact* supervision set, which comprises natural images and their VAE reconstructions, preserves semantics while altering pixel statistics. This yields matched pairs that remove semantic bias and isolate low-level discrepancies. By keeping both sets non-overlapping, the supervision remains *complementary yet independent*, aligning each model with its strength.

¹We sample semantically-implausible images from Echo-4o [47], an open-source collection of GPT-4o-conditioned surreal generations.

Fine-tuning of VLM and Expert. AlignGemini enforces task-model alignment by pairing models with their strengths: a VLM (e.g., Qwen2.5-VL [1]) for high-level semantic discrimination and an expert model (e.g., DINOv2) for low-level pixel-forensics discrimination. For VLM, we apply DPO on the semantically-implausible set described above. For the expert branch, we fine-tune on the pixel-artifact supervision set using strictly low-level supervision (no semantic labels). *This preserves supervision orthogonality and, by aligning each branch to its intended cue, prevents semantic leakage into the pixel expert and maintains task-model alignment.*

Dual-Perspective Detection of AlignGemini . At inference, AlignGemini adopts a dual-perspective scheme: the VLM branch performs *semantic* discrimination, while a pixel-artifact expert performs *low-level pixel artifact* discrimination. We apply an OR decision rule—an image is labeled synthetic if either branch flags it. The VLM, tailored to semantically inconsistent generations, remains robust to heavy post-processing, whereas the pixel-artifact expert targets subtle low-level artifacts and compensates for semantically faithful synthetic images. This complementary design yields comprehensive and robust detection.

5. Proposed Benchmark

AIGI-Now: An AIGI Detection Benchmark. We introduce *AIGI-Now*, a benchmark constructed from contemporary generators. As shown in Figure 4, AIGI-Now covers widely used modern models, including Nano Banana, GPT-

Table 1. Overall comparison of balanced accuracy on five in-the-wild benchmarks. The results of Forensic-Chat is cited from [24].

Method	Chameleon	WildRF				AIGI-Bench			CO-SPY-Bench/in-the-wild						BFree-Online	Avg.
		Facebook	Reddit	Twitter	Avg.	CommunityUI	SocialRF	Avg.	Civitai	DALL-E 3	instavibe.ai	Lexica	Midjourney-v6	Avg.		
NPR _{ECCV'24} [7]	59.9	78.1	61.0	51.3	63.5	54.2	58.6	56.4	0.2	4.5	0.4	4.6	82.5	18.4	40.4	47.7 ± 16.6
UnivFD _{CVPR'23} [27]	50.7	49.1	60.2	56.5	55.3	51.4	54.6	53.0	3.0	10.3	0.3	1.2	20.8	7.1	48.8	43.0 ± 18.1
FatFormer _{CVPR'24} [26]	51.2	54.1	68.1	54.4	58.9	51.9	55.4	53.7	0.0	1.7	0.0	2.8	32.2	7.3	50.0	44.2 ± 18.7
SAFE _{KDD'25} [20]	59.9	50.9	74.1	37.5	57.2	54.5	58.4	56.4	0.3	0.6	0.2	0.0	93.4	18.9	50.5	48.6 ± 15.2
C2P-CLIP _{AAAI'25} [31]	51.1	54.4	68.4	55.9	59.6	51.0	64.9	57.9	2.5	21.9	0.3	7.6	17.0	9.9	50.0	45.7 ± 18.3
AIDE _{ICLR'25} [44]	65.8	57.8	71.5	48.8	59.4	66.2	64.9	65.6	15.1	33.1	6.9	26.6	91.3	34.6	49.9	60.2 ± 13.1
DRCT _{ICML'24} [3]	56.6	90.3	65.7	82.3	79.4	54.8	54.0	54.4	51.9	90.8	85.3	99.6	76.1	<u>80.7</u>	56.1	65.4 ± 12.0
AlignedForensics _{ICLR'25} [30]	71.0	91.6	70.9	80.6	81.0	75.6	73.0	74.3	97.8	68.0	8.0	0.5	96.4	54.1	67.7	69.6 ± 8.9
CO-SPY _{CVPR'25} [5]	68.8	72.2	77.7	74.8	74.9	65.2	67.7	66.5	96.3	69.0	37.6	68.8	51.4	64.6	55.2	66.0 ± 6.4
Forensic-Chat (Qwen2.5-VL)[24]	-	77.8	83.4	82.1	81.1	74.6	89.8	<u>82.2</u>	-	-	-	-	-	-	-	-
BFree _{CVPR'25} [12]	<u>75.1</u>	94.7	<u>85.5</u>	97.9	<u>92.7</u>	<u>79.1</u>	84.8	81.9	<u>98.7</u>	<u>96.4</u>	14.3	50.5	<u>98.4</u>	71.7	<u>90.3</u>	<u>82.3</u> ± 9.2
Ours	85.5	<u>92.2</u>	90.9	<u>95.5</u>	92.9	91.9	<u>85.6</u>	88.8	100.0	99.6	<u>75.0</u>	<u>96.8</u>	99.9	94.3	97.5	91.8 ± 4.7 (+9.5)

Table 2. Overall comparison of balanced accuracy on proposed AIGI-Now datasets.

Method	Nano Banana		GPT-4o		Jimeng		Kling		Minimax		Flux Pro		Flux Krea		Flux Dev		Flux Kontext		Avg.	
	Pix	Sem	Pix	Sem	Pix	Sem	Pix	Sem	Pix	Sem	Pix	Sem	Pix	Sem	Pix	Sem	Pix	Sem	Pix	Sem
NPR _{CVPR'24} [7]	84.4	49.9	91.2	50.1	41.9	49.9	88.3	49.9	52.1	50.0	42.7	50.0	52.3	50.0	89.3	50.0	79.2	49.9	69.0 ± 21.2	50.0 ± 0.1
UnivFD _{CVPR'23} [27]	51.0	51.4	53.8	53.3	50.7	52.3	51.4	53.9	50.5	52.1	51.9	52.0	51.0	52.2	63.6	49.9	57.5	55.9	52.0 ± 2.3	52.6 ± 1.7
FatFormer _{CVPR'24} [26]	53.4	49.9	49.9	49.8	48.4	49.9	54.8	50.0	49.1	50.0	48.4	50.0	49.5	50.0	52.4	50.0	63.6	49.9	52.1 ± 4.8	49.9 ± 0.1
SAFE _{KDD'25} [20]	99.3	50.1	99.7	50.4	50.0	50.5	99.6	50.0	49.8	50.1	49.9	50.5	51.2	50.1	99.8	75.3	98.8	83.4	77.5 ± 25.9	56.7 ± 13.0
C2P-CLIP _{AAAT'25} [31]	50.0	50.0	49.8	50.0	49.8	50.0	50.7	49.9	50.3	50.0	52.0	50.0	50.1	50.0	52.6	50.0	60.7	50.0	51.7 ± 3.5	50.0 ± 0.0
AIDE _{ICLR'25} [44]	98.9	51.8	74.7	53.5	63.9	51.4	<u>98.2</u>	55.4	51.4	54.1	60.1	53.8	50.4	56.9	92.1	59.0	97.9	80.6	77.1 ± 21.4	57.4 ± 9.0
DRCT _{ICML'24} [3]	68.9	57.7	75.0	57.0	<u>89.3</u>	57.7	66.9	56.8	78.4	57.1	<u>83.0</u>	58.2	91.6	58.2	86.5	58.6	86.9	55.5	<u>80.7</u> ± 8.9	57.4 ± 0.9
AlignedForensics _{ICLR'25} [30]	88.0	50.3	50.8	50.8	82.1	50.0	69.6	50.2	56.7	50.3	65.5	49.9	59.5	50.1	78.6	50.2	65.0	50.0	68.4 ± 12.4	50.2 ± 0.2
CO-SPY _{CVPR'25} [5]	74.1	<u>58.3</u>	78.9	<u>63.1</u>	83.0	<u>76.2</u>	88.3	<u>78.8</u>	<u>77.9</u>	<u>65.6</u>	<u>77.3</u>	<u>72.7</u>	<u>89.1</u>	<u>74.0</u>	88.5	74.9	65.1	66.0	80.2 ± 7.9	<u>70.0</u> ± 6.9
BFree _{CVPR'25} [12]	69.6	52.8	59.2	56.7	75.6	54.5	86.1	60.7	56.2	49.9	71.8	54.5	59.5	51.5	74.8	54.5	77.1	53.4	70.0 ± 9.9	54.3 ± 3.1
Ours	96.0	95.6	<u>96.8</u>	95.7	96.2	95.6	97.3	94.9	91.3	89.8	89.9	93.2	83.0	92.6	96.6	95.3	86.6	88.0	92.6 ± 5.2 (+11.9)	93.4 ± 5.8 (+23.4)

Table 3. Overall comparison on three self-synthesized datasets.

Method	GenImage	DRCT-2M	AIGCDetectBenchmark	Avg.
NPR _{CVPR'24} [7]	51.5	37.3	53.1	47.3 ± 7.1
UnivFD _{CVPR'23} [27]	64.1	61.8	72.5	66.1 ± 4.6
FatFormer _{CVPR'24} [26]	62.8	52.2	85.0	66.7 ± 13.7
SAFE _{KDD'25} [20]	50.3	59.3	50.3	53.3 ± 4.2
C2P-CLIP _{AAAT'25} [31]	74.4	59.2	81.4	71.7 ± 9.3
AIDE _{ICLR'25} [44]	61.2	64.6	63.6	63.1 ± 1.4
DRCT _{ICML'24} [3]	84.7	90.5	81.4	85.5 ± 3.8
AlignedForensics _{ICLR'25} [30]	79.0	95.5	66.6	80.4 ± 11.8
CO-SPY _{CVPR'25} [5]	76.3	83.1	72.5	77.3 ± 5.4
BFree _{CVPR'25} [12]	<u>89.5</u>	99.1	88.2	<u>92.3</u> ± 6.0
Ours	91.7	<u>98.1</u>	<u>87.7</u>	92.5 ± 5.2 (+0.2)

4o, Jimeng, Kling, Minimax, Flux Pro, Flux Kera, Flux Kontext, Flux Dev. For each generator, we randomly sample 1,000 images from the COCO test set [25], extract their captions, and use the original caption and a deliberately surreal variant to synthesize both semantically faithful and semantically implausible images. Together with the corresponding real images, these form two subsets: (i) **semantically discriminative** samples, consisting of real images and surreal counterparts that are jointly subjected to aggressive post-processing to disrupt pixel statistics while preserving semantic mismatch, thereby forcing detectors to rely on semantic cues; and (ii) **pixel-artifact discriminative** samples, consisting of real and semantically-faithful synthetic images, minimizing semantic shortcuts and emphasizing low-level forensics. More details are in Appendix.

6. Experiments

Experimental setup. We evaluate methods on nine benchmarks grouped into three suites: (i) **five in-the-wild** benchmarks—Chameleon [44], WildRF [2], AIGI-Bench [21], Co-SPY-Bench/in-the-wild [5], and BFree-Online [12]; (ii) **AIGI-Now**; and (iii) **three self-synthesized** benchmarks—GenImage [54], DRCT-2M [3], and AIGCDetectBenchmark [51].

Table 4. Comparison on GenImage. Following BFree [12], synthetic images are JPEG-compressed to match real images’ format.

Method	Midjourney	SDv1.4	SDv1.5	ADM	GLIDE	Wukong	VQDM	BigGAN	Avg.
NPR _{CVPR'24} [7]	53.4	55.1	55.0	43.8	41.2	57.4	48.4	57.7	51.5 ± 6.3
UnivFD _{CVPR'23} [27]	55.1	55.6	55.7	62.5	61.3	61.1	76.9	84.4	64.1 ± 10.8
FatFormer _{CVPR'24} [26]	52.1	53.6	53.8	61.4	65.5	60.9	72.5	82.2	62.8 ± 10.4
SAFE _{KDD'25} [20]	49.0	49.7	49.8	49.5	53.0	50.3	50.2	50.9	50.3 ± 1.2
C2P-CLIP _{AAAT'25} [31]	56.6	77.5	76.9	71.6	73.5	79.4	73.7	85.9	74.4 ± 8.4
AIDE _{ICLR'25} [44]	58.2	77.2	77.4	50.4	54.6	70.5	50.8	50.6	61.2 ± 11.9
DRCT _{ICML'24} [3]	82.4	88.3	88.2	76.9	86.1	87.9	85.4	87.0	84.7 ± 2.7
AlignedForensics _{ICLR'25} [30]	97.5	99.7	99.6	52.4	57.6	99.6	75.0	50.6	79.0 ± 22.7
CO-SPY _{CVPR'25} [5]	58.5	63.1	69.8	72.5	81.6	92.5	82.2	90.3	76.3 ± 11.4
BFree _{CVPR'25} [12]	79.3	70.4	93.4	89.7	86.8	98.8	98.8	98.8	89.5 ± 9.3
Ours	<u>89.3</u>	<u>89.6</u>	<u>95.6</u>	<u>77.2</u>	90.3	98.3	<u>98.1</u>	<u>98.4</u>	91.7 ± 7.5 (+2.2)

Implementation Details. (i) *VLM*: Qwen2.5-VL-7B [1] is used as the VLM backbone and fine-tuned on a *pure semantic* set of 5,000 randomly sampled Unsplash [35] real images and 5,000 randomly sampled Echo-4o [47] synthetic images. During the DPO fine-tuning, we apply LoRA (rank = 16, $\alpha=32$), using learning rate 1×10^{-6} , batch size 8, and DPO coefficient $\beta=0.05$ for one epoch. (ii) *Expert branch*: we adopt a DINOv2 backbone with a classification head, fine-tuned using LoRA (rank = 8, $\alpha=1.0$) with learning rate 1×10^{-4} and batch size 16 on a pure pixel-artifact corpus constructed from VAE reconstructions: 11,8 k COCO training data paired with VAE-reconstructed data. At inference, an image is classified as real only if both the VLM and the expert predict real; otherwise, it is synthetic.

Evaluation Metrics and Comparative Methods. Balanced accuracy is adopted as the primary metric, defined as the mean of the real and fake accuracies. The competitive methods include NPR [7], FatFormer [26], UnivFD [27], SAFE [20], AIDE [44], C2P-CLIP [31], DRCT [3], AlignedForensics [30], CO-SPY [5], and BFree [12], Forensic-Chat [24]². All baselines are evaluated using their

²Other VLM detectors are excluded because (i) their training data domain-overlap with some benchmarks, compromising fairness, or (ii) their weights are not publicly released.

Table 5. Comparison of balanced accuracy on AIGCDetectBenchmark.

Method	ADM	DALLE2	GLIDE	Midjourney	VQDM	BigGAN	CycleGAN	GauGAN	ProGAN	SDXL	SD14	SD15	StarGAN	StyleGAN	StyleGAN2	WFR	Wukong	Avg.
NPR (CVPR'24) [7]	43.8	20.0	41.2	53.4	48.4	53.1	76.6	42.2	58.7	59.6	55.1	55.0	67.4	57.9	54.6	58.8	57.4	53.1 \pm 12.2
UnivFD (CVPR'23) [27]	62.5	50.0	61.3	55.1	76.9	87.5	96.9	98.8	99.4	58.2	55.6	55.7	95.1	80.0	69.4	69.2	61.1	72.5 \pm 17.3
FatFormer (CVPR'24) [26]	80.2	68.5	91.1	54.4	88.0	99.2	99.5	99.1	98.5	71.7	67.5	67.2	99.4	98.0	98.8	88.3	75.6	85.0 \pm 14.9
SAFE (KDD'25) [20]	49.5	49.5	53.0	49.0	50.2	52.2	51.9	50.0	50.0	49.8	49.7	49.8	50.1	50.0	50.0	49.8	50.3	50.3 \pm 1.1
C2P-CLIP (AAAI'25) [31]	71.6	52.3	73.5	56.6	73.7	98.4	96.8	98.8	99.3	62.3	77.5	76.9	99.6	93.1	93.1	79.4	94.8	81.4 \pm 15.6
AIDE (ICLR'25) [44]	52.9	51.1	60.2	49.8	69.3	70.1	93.6	60.6	89.0	49.6	51.6	51.0	72.1	66.5	59.0	80.6	54.5	63.6 \pm 13.9
DRCT (ICML'24) [3]	79.9	89.2	89.2	85.5	88.6	81.4	91.0	93.8	71.1	88.3	91.4	91.0	53.0	62.7	63.8	73.9	90.8	81.4 \pm 12.2
AlignedForensics (ICLR'25) [30]	51.6	52.0	55.6	96.2	72.1	51.2	49.5	50.8	50.7	95.1	99.7	99.6	53.8	52.7	51.6	50.0	99.6	66.6 \pm 21.6
CO-SPY (CVPR'25) [5]	58.5	84.9	81.7	69.8	72.6	70.5	53.5	68.1	74.0	81.4	92.5	92.2	62.8	60.0	60.1	60.9	90.2	72.5 \pm 12.6
BFree (CVPR'25) [12]	79.3	85.8	86.8	93.4	89.7	91.9	76.8	97.0	95.9	99.3	98.8	98.8	86.1	82.1	78.0	60.5	98.8	88.2 \pm 10.5
Ours	89.3	94.9	90.3	95.6	77.2	90.4	74.4	92.5	91.0	99.1	98.3	98.1	72.9	86.6	89.2	52.6	98.4	87.2 \pm 12.2 (-0.5)

Table 6. Comparison of balanced accuracy on DRCT-2M.

Method	LDM	SDv1.4	SDv1.5	SDv2	SDXL	SDXL-Refiner	SD-Turbo	SDXL-Turbo	LCM-SDv1.5	LCM-SDXL	SDv1-Ctrl	SDv2-Ctrl	SDXL-Ctrl	SDv1-DR	SDv2-DR	SDXL-DR	Avg.
NPR (CVPR'24) [7]	33.0	29.1	29.0	35.1	33.2	28.4	27.9	27.9	29.4	30.2	28.4	28.3	34.7	67.9	67.4	66.1	37.3 \pm 15.0
UnivFD (CVPR'23) [27]	85.4	56.8	56.4	58.2	63.2	55.0	56.5	53.0	54.5	65.9	68.0	65.4	75.9	64.6	56.2	53.9	61.8 \pm 8.9
FatFormer (CVPR'24) [26]	55.9	48.2	48.2	48.2	48.2	48.3	48.2	48.2	48.3	50.6	49.7	49.9	59.8	66.3	60.6	56.0	52.2 \pm 5.7
SAFE (KDD'25) [20]	50.3	50.1	50.0	50.0	49.9	50.1	50.0	50.0	50.1	50.0	49.9	50.0	54.7	98.2	98.5	97.3	59.3 \pm 19.2
C2P-CLIP (AAAI'25) [31]	83.0	51.7	51.7	52.9	51.9	64.6	51.7	50.6	52.0	66.1	56.9	54.7	77.8	67.2	57.1	56.7	59.2 \pm 9.9
AIDE (ICLR'25) [44]	64.4	74.9	75.1	58.5	53.5	66.3	52.8	52.8	70.0	54.3	65.9	53.6	53.9	95.3	73.3	69.0	64.6 \pm 11.8
DRCT (ICML'24) [3]	96.7	96.3	96.3	94.9	96.2	93.5	93.4	92.9	91.2	95.0	95.6	92.7	92.0	94.1	69.6	57.4	90.5 \pm 7.4
AlignedForensics (ICLR'25) [30]	99.9	99.9	99.9	99.6	90.2	81.3	99.7	89.4	99.7	90.0	99.9	99.2	87.6	99.9	99.8	92.6	95.5 \pm 6.1
CO-SPY (CVPR'25) [5]	72.2	99.4	82.4	99.3	73.7	96.7	70.9	97.2	94.8	51.0	51.5	99.4	99.4	50.7	83.9	91.1	83.1 \pm 16.7
BFree (CVPR'25) [12]	99.5	99.3	99.3	99.3	99.5	99.0	99.5	98.0	99.4	99.4	99.4	99.4	99.4	96.4	99.9	99.2	99.1 \pm 0.8
Ours	99.1	98.7	98.8	98.2	98.0	98.9	97.7	94.6	96.4	98.3	98.6	99.0	99.2	98.9	99.2	96.2	98.1 \pm 1.3 (-1.0)

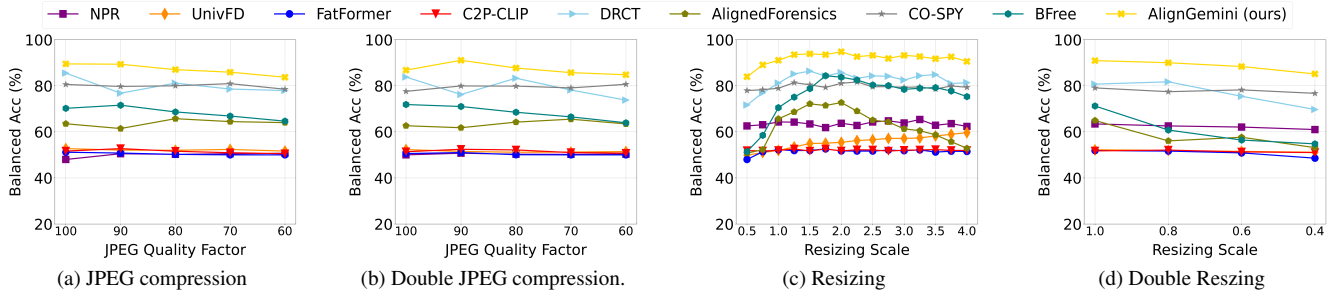


Figure 5. Robustness evaluation on AIGI-Now (pixel). Double JPEG compression applies JPEG compression with the same quality factor twice. Double resizing first downsamples the image and then upsamples it to the original size. The results show that our AlignGemini consistently exhibits superior robustness consistently under these post-processing operations.

officially released checkpoints, without per-benchmark re-tuning. For AlignGemini, across all benchmarks, we uniformly adopt a single fine-tuned Qwen2.5-VL-7B as the semantic branch and a DINOv2-based expert as the pixel-artifact branch. We organize our experimental results around three key questions:

Q1. Does AlignGemini achieve stronger generalization?

Comparison on five in-the-wild benchmarks. Table 1 reports the performance on five in-the-wild benchmarks³. These benchmarks consist of Internet-sourced images generated by unknown models and processed with unknown pipelines, placing them out of distribution for all detectors and providing a faithful test of real-world generalization. In this challenging regime, most baselines achieve accuracies below 70, underscoring the difficulty. AlignGemini consistently surpasses all baselines, improving accuracy by **+9.5**, demonstrating its superior generalization.

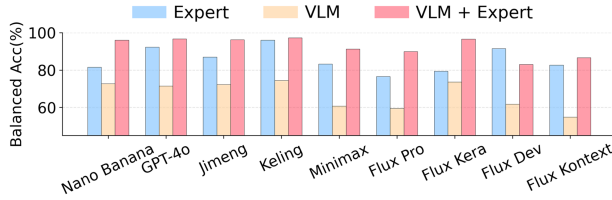
³Results on CO-SPY-Bench/in-the-wild may differ from those reported in the original papers because the full in-the-wild set is not publicly available due to licensing restrictions; our evaluation is conducted on the subset provided by the CO-SPY authors.

Comparison on AIGI-Now Benchmark. Table 2 compares detectors on **AIGI-Now**, a benchmark designed to assess both pixel-level and semantic detection of images from the latest generators. Existing detectors show poor pixel-level generalization: only DRCT and CO-SPY exceed 80 accuracy, while most baselines exhibit severe degradation. In contrast, AlignGemini improves pixel accuracy by **+11.9**, demonstrating strong generalization to modern generators’ pixel cues. Notably, this gain is not attributable to domain overlap, as AlignGemini is trained solely on heavily post-processed GPT-4o images and SD2.1 VAE that are out-of-domain w.r.t. AIGI-Now. For semantic detection, almost all detectors fail to capture semantic flaws, with average accuracies below 70, whereas AlignGemini achieves a non-trivial accuracy of **93.4**. Together, these results show that existing detectors are fragile under aggressive post-processing and often miss evident semantic flaws, whereas AlignGemini leverages complementary cues to achieve stronger generalization.

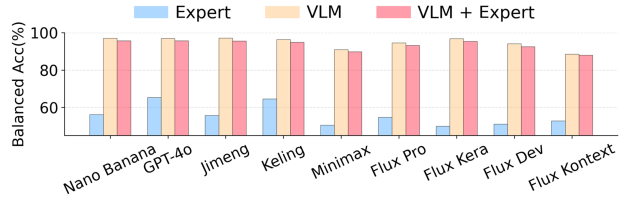
Comparison on three self-synthesized benchmarks. Table 3 summarizes the results on three self-synthesized benchmarks, with per-benchmark details reported in Tables 4–6. GenImage and DRCT-2M are dominated by

Table 7. Evaluate the in-the-wild accuracies and FLUX-specific accuracies of AlignGemini when upgrading the VLM backbone and the pixel experts. **SD/FLUX** denote experts trained on SD2/FLUX VAE-reconstructed images, respectively. **SD+FLUX** uses both experts jointly. The results show that performance consistently improves with stronger backbones and additional experts.

Method			In-the-wild benchmarks						AIGI-Now					
			Chameleon	WildRF	AIGI-Bench	CO-SPY-Bench/in-the-wild	BFree-Online	Avg.	Flux Pro.	Flux Kera.	Flux Dev	Flux Kontext.	Avg.	
Baseline	Qwen2.5-VL-7B (Untrained)	-	59.1	83.8	75.7	57.4	77.6	74.1 \pm 11.8	69.6	67.7	73.3	66.9	69.4 \pm 2.9	
	CO-SPY	-	68.8	74.9	66.5	64.6	55.2	66.0 \pm 6.4	75.0	81.5	81.7	65.6	75.9 \pm 7.6	
	BFree	-	75.1	92.7	81.9	71.7	90.3	82.3 \pm 9.2	63.1	55.5	64.6	65.3	62.1 \pm 4.5	
Ours	Qwen2.5-VL-7B	SD	85.5	92.9	88.8	94.3	97.5	91.8 \pm 4.7 (+9.5)	91.5	87.7	95.9	87.3	90.6 \pm 4.0 (+14.7)	
	Qwen2.5-VL-7B	SD + FLUX	85.6	93.1	88.9	94.3	97.5	91.9 \pm 4.7 (+9.6)	91.5	92.1	96.5	89.2	92.3 \pm 3.1 (+16.4)	
	Qwen3-VL-32B	SD	87.9	93.9	90.4	96.0	95.3	92.7 \pm 3.4 (+10.4)	89.7	83.6	95.5	87.1	88.9 \pm 3.0 (+13.0)	
	Qwen3-VL-32B	SD + FLUX	88.4	94.4	90.8	96.3	95.6	93.1 \pm 3.4 (+10.8)	89.8	90.5	96.4	89.1	91.4 \pm 3.4 (+15.5)	
	Qwen3-VL-235B	SD	89.8	94.0	91.2	97.2	97.8	94.0 \pm 3.5 (+11.7)	93.1	89.9	97.0	87.8	92.0 \pm 4.0 (+16.1)	
	Qwen3-VL-235B	SD + FLUX	90.3	94.5	91.6	97.5	98.2	94.4 \pm 3.5 (+12.1)	93.2	94.0	97.6	89.8	93.7 \pm 3.2 (+17.8)	



(a) AIGI-Now (pixel-level discriminative samples)



(b) AIGI-Now (semantically discriminative samples)

Figure 6. Isolated impact of VLM and expert branches. (a) Evaluates pixel-artifact detection. (b) Evaluates semantic detection.

diffusion-based images, whereas AIGCDetectBenchmark primarily contains GAN-generated images. Across these benchmarks, AlignGemini outperforms competing methods in terms of average accuracy. Notably, its superior performance on AIGCDetectBenchmark, achieved without using any GAN-generated images during training, demonstrates strong cross-architecture generalization.

Q2. Does AlignGemini exhibit higher robustness?

Comparison on Robustness. Figure 5 evaluates the robustness under four post-processing operations. Existing pixel-artifact detectors (e.g., NPR) are highly vulnerable: most of them degrade sharply under double resizing with scale factor 0.4, where neighboring pixels are largely re-generated and original pixel statistics are severely disrupted. In contrast, detectors incorporating semantic features (e.g., CO-SPY) are more stable. Remarkably, AlignGemini consistently attains the strongest robustness, as its complementary use of semantic and pixel-level cues substantially enhances resilience to post-processing.

Q3. Is AlignGemini extensible?

Extensibility of AlignGemini. The extensibility is a key consideration for practical deployment. As shown in Table 7, we demonstrate two complementary ways to further extend AlignGemini. **VLM branch:** scaling the backbone from Qwen2.5-VL-7B to Qwen3-VL-235B improves accuracy on Chameleon from 85.5 to 90.3, indicating that stronger VLM backbones are an effective extension path. **Expert branch:** incorporating an additional expert model trained on FLUX VAE reconstructions further enhances performance, particularly for FLUX-generated images. These results confirm the extensibility of AlignGemini, and the two proposed extensions are easy to deploy.

Table 8. Comparison with baseline methods under the same training set as AlignGemini, isolating the effect of data advantage.

Method	Chameleon	WildRF	AIGI-Bench	CO-SPY-Bench/in-the-wild	BFree-Online	Avg.
UnivFD	52.0	63.2	58.2	18.9	49.8	55.8 \pm 17.3
AIDE	64.2	61.3	63.2	44.2	50.2	56.6 \pm 8.9
CO-SPY	66.7	70.2	65.4	52.6	53.0	61.2 \pm 8.0
NPR	58.3	56.9	54.2	12.3	48.9	46.1 \pm 19.2
SAFE	61.2	62.4	55.3	21.7	52.6	50.6 \pm 16.7
DINOv2-ViT-L-14	51.7	57.8	57.8	13.4	49.2	54.1 \pm 18.6
Qwen2.5-VL-7B	65.7	86.3	80.4	67.6	82.2	76.6 \pm 9.3
Ours	85.5	92.9	88.8	94.3	97.5	91.8 \pm 4.7 (+15.2)

6.1. Ablation study

Ablation on each module. Figure 6 quantifies the contributions of AlignGemini’s two branches. Panel (a) shows that removing the VLM sharply degrades semantic detection, while panel (b) shows that removing the expert impairs pixel-level detection. Only the integrated model generalizes robustly across both tasks.

Ablation on data advantage. A natural concern is that our gains might arise from using more data. We therefore retrain all baselines on identical corpora comprising the same semantic and pixel-artifact supervision sets. As shown in Table 8, AlignGemini still yields a **+15.2** improvement. These supports *task-model alignment*: semantic-only supervision trains the VLM, and pure pixel-artifact supervision trains the expert. By contrast, forcing a single model to learn from mixed supervision dilutes both signals.

7. Conclusion

We identify *task-model misalignment* as a primary cause of VLM-based detectors’ underperformance and formalize the *Task-Model Alignment* principle. We develop **AlignGemini**, a dual-perspective detector that couples semantic signals from a VLM with pixel-level forensics from a specialist expert. Extensive experiments show improved generalization, robustness, and extensibility: AlignGemini improves the in-the-wild accuracy by **+9.5** despite training on a sim-

plified corpus. We also release **AIGI-Now**, a benchmark for closer-to-real-world evaluation across contemporary commercial generators. Together, Task-Model Alignment principle and AIGI-Now benchmark advance AIGI detection toward reliable real-world practice.

References

- [1] Shuai Bai, Keqin Chen, Xuejing Liu, Jialin Wang, Wenbin Ge, Sibao Song, Kai Dang, Peng Wang, Shijie Wang, Jun Tang, et al. Qwen2. 5-vl technical report. *arXiv preprint arXiv:2502.13923*, 2025. 5, 6
- [2] Bar Cavia, Eliahu Horwitz, Tal Reiss, and Yedid Hoshen. Real-time deepfake detection in the real-world. *arXiv preprint arXiv:2406.09398*, 2024. 6
- [3] Baoying Chen, Jishen Zeng, Jianquan Yang, and Rui Yang. Drc: Diffusion reconstruction contrastive training towards universal detection of diffusion generated images. In *Forty-first International Conference on Machine Learning*, 2024. 6, 7
- [4] Yize Chen, Zhiyuan Yan, Guangliang Cheng, Kangran Zhao, Siwei Lyu, and Baoyuan Wu. X2-dfd: A framework for explainable and extendable deepfake detection. *arXiv preprint arXiv:2410.06126*, 2024. 2, 3
- [5] Siyuan Cheng, Lingjuan Lyu, Zhenting Wang, Xiangyu Zhang, and Vikash Sehwal. Co-spy: Combining semantic and pixel features to detect synthetic images by ai. In *Proceedings of the Computer Vision and Pattern Recognition Conference*, pages 13455–13465, 2025. 3, 6, 7
- [6] Beilin Chu, Xuan Xu, Xin Wang, Yufei Zhang, Wei-ke You, and Linna Zhou. Fire: Robust detection of diffusion-generated images via frequency-guided reconstruction error. In *CVPR*, 2025. 2
- [7] Davide Cozzolino, Giovanni Poggi, Matthias Nießner, and Luisa Verdoliva. Zero-shot detection of ai-generated images. In *European Conference on Computer Vision*, pages 54–72. Springer, 2024. 3, 6, 7
- [8] Yueying Gao, Dongliang Chang, Bingyao Yu, Haotian Qin, Lei Chen, Kongming Liang, and Zhanyu Ma. Fakereasoning: Towards generalizable forgery detection and reasoning. *arXiv preprint arXiv:2503.21210*, 2025. 2
- [9] Zorik Gekhman, Gal Yona, Roei Aharoni, Matan Eyal, Amir Feder, Roi Reichart, and Jonathan Herzig. Does fine-tuning llms on new knowledge encourage hallucinations? *arXiv preprint arXiv:2405.05904*, 2024. 2
- [10] Ian J Goodfellow et al. Generative adversarial nets. In *Advances in Neural Information Processing Systems*, 2014. 2
- [11] Rynaa Grover, Jayant Sravan Tamarapalli, Sahiti Yerramilli, and Nilay Pande. Huemany: Probing fine-grained visual perception in mllms. *arXiv preprint arXiv:2506.03194*, 2025. 3
- [12] Fabrizio Guillaro, Giada Zingarini, Ben Usman, Avneesh Sud, Davide Cozzolino, and Luisa Verdoliva. A bias-free training paradigm for more general ai-generated image detection. *arXiv preprint arXiv:2412.17671*, 2024. 6, 7
- [13] Jonathan Ho et al. Denoising diffusion probabilistic models. *Advances in Neural Information Processing Systems*, 33:6840–6851, 2020. 2
- [14] Tai-Ming Huang, Wei-Tung Lin, Kai-Lung Hua, Wen-Huang Cheng, Junichi Yamagishi, and Jun-Cheng Chen. Thinkfake: Reasoning in multimodal large language models for ai-generated image detection. *arXiv preprint arXiv:2509.19841*, 2025. 2
- [15] Yikun Ji, Yan Hong, Jiahui Zhan, Haoxing Chen, Huijia Zhu, Weiqiang Wang, Liqing Zhang, Jianfu Zhang, et al. Towards explainable fake image detection with multi-modal large language models. *arXiv preprint arXiv:2504.14245*, 2025. 2, 3
- [16] Shan Jia, Reilin Lyu, Kangran Zhao, Yize Chen, Zhiyuan Yan, Yan Ju, Chuanbo Hu, Xin Li, Baoyuan Wu, and Siwei Lyu. Can chatgpt detect deepfakes? a study of using multimodal large language models for media forensics. In *Proceedings of the IEEE/CVF Conference on Computer Vision and Pattern Recognition*, pages 4324–4333, 2024. 3
- [17] Hengrui Kang, Siwei Wen, Zichen Wen, Junyan Ye, Weijia Li, Peilin Feng, Baichuan Zhou, Bin Wang, Dahua Lin, Linfeng Zhang, et al. Legion: Learning to ground and explain for synthetic image detection. *arXiv preprint arXiv:2503.15264*, 2025. 2, 3
- [18] Dimitrios Karageorgiou, Symeon Papadopoulos, Ioannis Kompatsiaris, and Efstratios Gavves. Any-resolution ai-generated image detection by spectral learning. In *CVPR*, 2025. 2
- [19] Andrew K Lampinen, Arslan Chaudhry, Stephanie CY Chan, Cody Wild, Diane Wan, Alex Ku, Jörg Bornschein, Razvan Pascanu, Murray Shanahan, and James L McClelland. On the generalization of language models from in-context learning and finetuning: a controlled study. *arXiv preprint arXiv:2505.00661*, 2025. 2
- [20] Ouxiang Li, Jiayin Cai, Yanbin Hao, Xiaolong Jiang, Yao Hu, and Fuli Feng. Improving synthetic image detection towards generalization: An image transformation perspective. *arXiv preprint arXiv:2408.06741*, 2024. 2, 6, 7
- [21] Ziqiang Li, Jiazhen Yan, Ziwen He, Kai Zeng, Weiwei Jiang, Lizhi Xiong, and Zhangjie Fu. Is artificial intelligence generated image detection a solved problem? *arXiv preprint arXiv:2505.12335*, 2025. 6
- [22] Z. Li, J. Yan, Z. He, et al. Is artificial intelligence generated image detection a solved problem? *arXiv preprint arXiv:2505.12335*, 2025. 3
- [23] Kaiqing Lin, Yuzhen Lin, Weixiang Li, Taiping Yao, and Bin Li. Standing on the shoulders of giants: Reprogramming visual-language model for general deepfake detection. In *Proceedings of the AAAI Conference on Artificial Intelligence*, pages 5262–5270, 2025. 2
- [24] Kaiqing Lin, Zhiyuan Yan, Ruoxin Chen, Junyan Ye, Ke-Yue Zhang, Yue Zhou, Peng Jin, Bin Li, Taiping Yao, and Shouhong Ding. Seeing before reasoning: A unified framework for generalizable and explainable fake image detection. *arXiv preprint arXiv:2509.25502*, 2025. 3, 6
- [25] Tsung-Yi Lin, Michael Maire, Serge Belongie, James Hays, Pietro Perona, Deva Ramanan, Piotr Dollár, and C Lawrence Zitnick. Microsoft coco: Common objects in context. In *European conference on computer vision*, pages 740–755. Springer, 2014. 6
- [26] Huan Liu, Zichang Tan, Chuangchuang Tan, Yunchao Wei, Jingdong Wang, and Yao Zhao. Forgery-aware adaptive

- transformer for generalizable synthetic image detection. In *Proceedings of the IEEE/CVF Conference on Computer Vision and Pattern Recognition*, pages 10770–10780, 2024. 2, 6, 7
- [27] Utkarsh Ojha et al. Towards universal fake image detectors that generalize across generative models. In *Proceedings of the IEEE/CVF Conference on Computer Vision and Pattern Recognition*, pages 24480–24489, 2023. 2, 6, 7
- [28] Siran Peng, Zipei Wang, Li Gao, Xiangyu Zhu, Tianshuo Zhang, Ajian Liu, Haoyuan Zhang, and Zhen Lei. Mllm-enhanced face forgery detection: A vision-language fusion solution. *arXiv preprint arXiv:2505.02013*, 2025. 2
- [29] Alec Radford et al. Learning transferable visual models from natural language supervision. In *International Conference on Machine Learning*, pages 8748–8763. PMLR, 2021. 2
- [30] Anirudh Sundara Rajan, Utkarsh Ojha, Jedidiah Schloesser, and Yong Jae Lee. Aligned datasets improve detection of latent diffusion-generated images, 2025. 6, 7
- [31] Chuangchuang Tan, Renshuai Tao, Huan Liu, Guanghua Gu, Baoyuan Wu, Yao Zhao, and Yunchao Wei. C2p-clip: Injecting category common prompt in clip to enhance generalization in deepfake detection. In *Proceedings of the AAAI Conference on Artificial Intelligence*, 2024. 2, 6, 7
- [32] Chuangchuang Tan, Yao Zhao, Shikui Wei, Guanghua Gu, Ping Liu, and Yunchao Wei. Frequency-aware deepfake detection: Improving generalizability through frequency space domain learning. In *Proceedings of the AAAI Conference on Artificial Intelligence*, pages 5052–5060, 2024.
- [33] Chuangchuang Tan, Yao Zhao, Shikui Wei, Guanghua Gu, Ping Liu, and Yunchao Wei. Rethinking the up-sampling operations in cnn-based generative network for generalizable deepfake detection. In *Proceedings of the IEEE/CVF Conference on Computer Vision and Pattern Recognition*, pages 28130–28139, 2024. 2
- [34] Chuangchuang Tan, Jinglu Wang, Xiang Ming, Renshuai Tao, Yunchao Wei, Yao Zhao, and Yan Lu. Forenx: Towards explainable ai-generated image detection with multimodal large language models. *arXiv preprint arXiv:2508.01402*, 2025. 2
- [35] Unsplash. Unsplash. <https://unsplash.com/data>, 2025. 6
- [36] Aäron Van Den Oord, Nal Kalchbrenner, and Koray Kavukcuoglu. Pixel recurrent neural networks. In *International conference on machine learning*, pages 1747–1756. PMLR, 2016. 2
- [37] Sheng-Yu Wang et al. Cnn-generated images are surprisingly easy to spot... for now. In *Proceedings of the IEEE/CVF Conference on Computer Vision and Pattern Recognition*, pages 8695–8704, 2020. 2
- [38] Haiquan Wen, Tianxiao Li, Zhenglin Huang, Yiwei He, and Guangliang Cheng. Busterrx+: Towards unified cross-modal ai-generated content detection and explanation with mllm. *arXiv preprint arXiv:2507.14632*, 2025. 3
- [39] Siwei Wen, Junyan Ye, Peilin Feng, Hengrui Kang, Zichen Wen, Yize Chen, Jiang Wu, Wenjun Wu, Conghui He, and Weijia Li. Spot the fake: Large multimodal model-based synthetic image detection with artifact explanation. *arXiv preprint arXiv:2503.14905*, 2025. 2
- [40] Cheng Xia, Manxi Lin, Jiexiang Tan, Xiaoxiong Du, Yang Qiu, Junjun Zheng, Xiangheng Kong, Yuning Jiang, and Bo Zheng. Mirage: Towards ai-generated image detection in the wild. *arXiv preprint arXiv:2508.13223*, 2025. 2
- [41] Zhipei Xu, Xuanyu Zhang, Runyi Li, Zecheng Tang, Qing Huang, and Jian Zhang. Fakeshield: Explainable image forgery detection and localization via multi-modal large language models. In *The Thirteenth International Conference on Learning Representations*, 2025. 2
- [42] Zhipei Xu, Xuanyu Zhang, Xing Zhou, and Jian Zhang. Avatarshield: Visual reinforcement learning for human-centric video forgery detection. *arXiv preprint arXiv:2505.15173*, 2025. 2, 3
- [43] Hao Yan, Handong Zheng, Hao Wang, Liang Yin, Xingchen Liu, Zhenbiao Cao, Xinxing Su, Zihao Chen, Jihao Wu, Minghui Liao, et al. Visuriddles: Fine-grained perception is a primary bottleneck for multimodal large language models in abstract visual reasoning. *arXiv preprint arXiv:2506.02537*, 2025. 2
- [44] Shilin Yan, Ouxiang Li, Jiayin Cai, Yanbin Hao, Xiaolong Jiang, Yao Hu, and Weidi Xie. A sanity check for ai-generated image detection. *arXiv preprint arXiv:2406.19435*, 2024. 3, 6, 7
- [45] Zhiyuan Yan, Jiangming Wang, Peng Jin, Ke-Yue Zhang, Chengchun Liu, Shen Chen, Taiping Yao, Shouhong Ding, Baoyuan Wu, and Li Yuan. Orthogonal subspace decomposition for generalizable ai-generated image detection. In *Forty-second International Conference on Machine Learning*. 2
- [46] Zhiyuan Yan, Kaiqing Lin, Zongjian Li, Junyan Ye, Hui Han, Zhendong Wang, Hao Liu, Bin Lin, Hao Li, Xue Xu, et al. Can understanding and generation truly benefit together—or just coexist? *arXiv preprint arXiv:2509.09666*, 2025. 2
- [47] Junyan Ye, Dongzhi Jiang, Zihao Wang, Leqi Zhu, Zhenghao Hu, Zilong Huang, Jun He, Zhiyuan Yan, Jinghua Yu, Hongsheng Li, et al. Echo-4o: Harnessing the power of gpt-4o synthetic images for improved image generation. *arXiv preprint arXiv:2508.09987*, 2025. 5, 6
- [48] Heeji Yoon, Jaewoo Jung, Junwan Kim, Hyungyu Choi, Heeseong Shin, Sangbeom Lim, Honggyu An, Chaehyun Kim, Jisang Han, Donghyun Kim, et al. Visual representation alignment for multimodal large language models. *arXiv preprint arXiv:2509.07979*, 2025. 3
- [49] Wayne Zhang, Changjiang Jiang, Zhonghao Zhang, Chenyang Si, Fengchang Yu, and Wei Peng. Ivy-fake: A unified explainable framework and benchmark for image and video aigc detection. *arXiv preprint arXiv:2506.00979*, 2025. 2, 3
- [50] Chende Zheng, Chenhao Lin, Zhengyu Zhao, Hang Wang, Xu Guo, Shuai Liu, and Chao Shen. Breaking semantic artifacts for generalized ai-generated image detection. *Advances in Neural Information Processing Systems*, 37:59570–59596, 2024. 2
- [51] Nan Zhong, Yiran Xu, Sheng Li, Zhenxing Qian, and Xinpeng Zhang. Patchcraft: Exploring texture patch for efficient ai-generated image detection. *arXiv preprint arXiv:2311.12397*, pages 1–18, 2024. 6

- [52] Yue Zhou, Bing Fan, Pradeep K. Atrey, and Feng Ding. Exposing deepfakes using dual-channel network with multi-axis attention and frequency analysis. In *Proceedings of the 2023 ACM Workshop on Information Hiding and Multimedia Security*, pages 169–174, 2023. [2](#)
- [53] Ziyin Zhou, Yunpeng Luo, Yuanchen Wu, Ke Sun, Jiayi Ji, Ke Yan, Shouhong Ding, Xiaoshuai Sun, Yunsheng Wu, and Rongrong Ji. Aigi-holmes: Towards explainable and generalizable ai-generated image detection via multimodal large language models. *arXiv preprint arXiv:2507.02664*, 2025. [2](#)
- [54] Mingjian Zhu, Hanting Chen, Qiangyu Yan, Xudong Huang, Guanyu Lin, Wei Li, Zhijun Tu, Hailin Hu, Jie Hu, and Yunhe Wang. Genimage: A million-scale benchmark for detecting ai-generated image. *Advances in Neural Information Processing Systems*, 36:77771–77782, 2023. [6](#)